

Shape statistics of Sloan Digital Sky Survey superclusters

Spyros Basilakos¹.

¹ *Institute of Astronomy & Astrophysics, National Observatory of Athens, I. Metaxa & V. Pavlou, Palaia Penteli, 15236 Athens, Greece*

15 June 2018

ABSTRACT

We study the supercluster shape properties of the recently compiled SDSS cluster catalog using an approach based on differential geometry. We detect superclusters by applying the percolation algorithm to observed cluster populations, extended out to $z_{\max} \leq 0.23$ in order to avoid selection biases. We utilize a set of shapefinders in order to study the morphological features of superclusters with ≥ 8 cluster members and find that filamentary morphology is the dominant supercluster shape feature, in agreement with previous studies.

Keywords: cosmology: theory - clusters - superclusters: general - large-scale structure of universe - Optical: clusters

1 INTRODUCTION

The launch of the recent observational data has brought great progress in understanding the cosmic structure formation pattern. From the large scale structure point of view it has been shown that cluster of galaxies are not randomly distributed but tend to aggregate in larger groups, the so called superclusters (cf. Bahcall 1988). Since they have been seeded by density perturbations of the largest scale ($\sim 100 h^{-1}\text{Mpc}$), they therefore constitute objects with which one can study the details of the fluctuations that gave rise to cosmic structures (cf. West 1989; Einasto et al. 1997). In this framework, we can extract useful information regarding the evolution of the large-scale structure of the universe and test cosmological models within the framework of hierarchical structure formation scenario (Bahcall & Soneira 1984; Bahcall 1988; Frisch et al. 1995).

Indeed many authors have confirmed that the large scale clustering pattern of galaxies is described well by a filamentary distribution (Zel'dovich, Einasto & Shandarin 1982; de Lapparent, Geller & Huchra 1991; Einasto et al. 2001). However, only recently (Sathyaprakash et al. 1998a; Basilakos, Plionis & Rowan-Robinson 2001; Kolokotronis, Basilakos & Plionis 2002) was any significance given to cosmological inferences from supercluster shape statistics claiming that a low matter density ($\Omega_m = 1 - \Omega_\Lambda = 0.3$) flat cosmological model (ΛCDM) fits the observational results at high significance level. Sathyaprakash et al. (1998a) and Basilakos et al. (2001) have used infrared galaxy samples (1.2 Jy and PSCz, respectively), whereas Kolokotronis, et al. (2002) considered Abell/ACO clusters.

A variety of geometrical and topological methods have been developed and applied to observational data in order to give qualitative and quantitative description

of large scale structure (cf. Weinberg, Gott & Melott 1987; Coles & Plionis 1991; Mecke et al. 1994; Sahni & Coles 1995; Yess & Shandarin 1996; Kerscher et al. 1997; Kerscher et al. 2001a, b; Hoyle, Vogeley & Gott 2002; Hoyle et al. 2003; Jatush et al. 2003 and references therein). Recently, a new technique was obtained by Sahni, Sathyaprakash & Shandarin (1998) based on the differential geometry (Minkowski functionals), in order to describe in detail the geometrically and topologically complex features of large scale structure. In its general form the Minkowski functionals have been shown to provide a better approximation to complex structures than the simple semi-axes procedures (Sathyaprakash, Sahni & Shandarin 1998b). For example, in cases where the matter distribution is one-dimensional but not along straight line, one is bound to get somewhat smaller signal for filamentarity from the Babul & Starkman (1992) and Luo & Vishniac (1995) statistics (semi-axes method). This problem is even more true for two dimensional structures.

The first time this new shapefinder technique was applied to astronomical data was in Basilakos et al. (2001), where it ascertained that the prominent feature of the large scale structures we see today is filamentarity, as it has also been observed in N-body simulations of gravitational clustering (Sathyaprakash et al. 1998b and references therein). In this paper we utilize the recently completed SDSS CE cluster catalog (Goto et al. 2002) in order: (i) to study whether we can reliably identify SDSS superclusters and measure their shape and size distribution and (ii) whether or not superclusters verify the dominance of filamentarity as the basic trait of large scale structure. A different analysis applied by Einasto et al. (2002), who identified clusters and 43 superclusters (high density regions) from the smoothed galaxy density

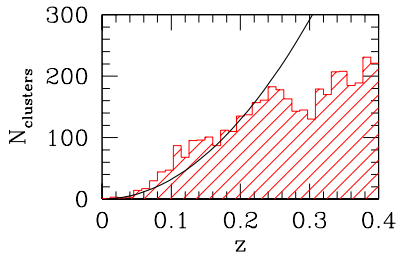


Figure 1. The estimated (histogram) and the expected (line) number of the SDSS clusters as a function of redshift.

field of the SDSS Early Data Release (Stoughton et al. 2002) catalog. The plan of the paper is as follows. The observed dataset is presented in section 2. In section 3, we give a brief report on the method used to investigate supercluster shape properties and comment on the systematic effects introduced in our analysis. In section 4, we present the morphological parameters of the SDSS superclusters data and finally in section 5 we draw our conclusions.

2 THE SDSS CLUSTER CATALOGUE

In the present analysis we use the recent SDSS CE cluster catalog (Goto et al. 2002), which contains 2770 and 1868 galaxy clusters in the North ($145.1^\circ < RA < 236.0^\circ$, $-1.25^\circ < DEC < 1.25^\circ$) and South ($350.5^\circ < RA < 56.61^\circ$, $-1.25^\circ < DEC < 1.25^\circ$) slices respectively, covering an area of $\sim 400\text{deg}^2$ in the sky. Redshifts are converted to proper distances using a spatially flat cosmology with $H_0 = 100h \text{ km s}^{-1} \text{ Mpc}^{-1}$ and $\Omega_m = 1 - \Omega_\Lambda = 0.3$. In figure 1, we present the estimated (histogram) and the expected (line) number of the SDSS clusters as a function of redshift. It is obvious that up to redshift $z_{\text{max}} \leq 0.23$ we have a volume limited sample due to the fact that the number of the SDSS clusters is proportional to r^3 . We have compared the two distributions (up to $z_{\text{max}} \leq 0.23$) via a standard Kolmogorov-Smirnov (KS) statistical test and the corresponding probability of consistency between model and observations is $\mathcal{P}_{\text{KS}} \simeq 0.43$. Therefore, the redshift cutoff corresponds to a limiting distance $r_{\text{max}} \leq 653h^{-1} \text{ Mpc}$. This subsample contains 1690 entries in the North and South slices respectively.

In order to investigate further the latter result we need to compute the number density of the cluster sample as a function of redshift. We do so by using five equal volume shells ($\delta V \approx 2.4 \times 10^6 h^{-3} \text{ Mpc}^3$) up to $z_{\text{max}} \leq 0.23$ and calculate, as a function of redshift, the cluster space density (continuous line in figure 2). While, the corresponding average-over-shells density for the SDSS subsample is $n_{\text{SDSS}}(\leq z_{\text{max}}) \simeq 1.26(\pm 0.32) \times 10^{-4} h^3 \text{ Mpc}^{-3}$ (see dashed line in figure 2) giving rise to intercluster separation of order $\sim 20 \pm 1.47 h^{-1} \text{ Mpc}$.

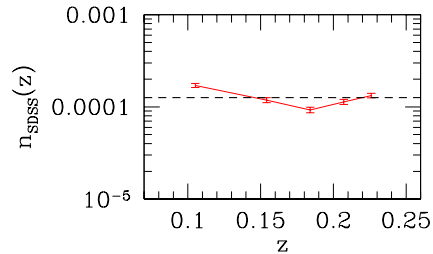


Figure 2. The SDSS cluster space density (continuous line) estimated in equal-volume shells with its Poissonian uncertainty. While the dashed line is the average $n_{\text{SDSS}}(z \leq 0.23) \simeq 1.26 \times 10^{-4} h^3 \text{ Mpc}^{-3}$.

3 SHAPE STATISTIC

3.1 SDSS Superclusters

Identifying real superclusters is a difficult problem in general, due to observational selection function, that can significantly affect the visual structure of superclusters and distort the true pattern. Our supercluster finding algorithm consists of the main steps: The supercluster catalogs constructed by utilizing, in supergalactic coordinates, a constant size neighborhood radius, i.e. the percolation radius (Zel'dovich et al. 1982). In particular, we place a sphere of a certain size around each cluster and then find all neighboring spheres having an overlap region. Then, all mutually linked clusters are joined together to form groups (with k members), and the groups with more than $k \geq 8$ clusters are identified as candidate rich superclusters. Of course, we choose the optimal percolation radius, by repeating the procedure by successively increasing the size of the sphere. At the end, we identify the radius that yields the maximum number of superclusters, which obviously occurs before the percolation of the superclusters themselves. Performing many tests we select a percolation radius $R_{\text{pr}} \simeq 26h^{-1} \text{ Mpc}$ following the same criteria to those of Einasto et al. (2001; Kolokotronis et al. 2002 and references therein). To this end this procedure produced a list of 57 rich superclusters.

3.2 Test for systematic errors

In this section we investigate the number of the random clumps revealed from the percolation procedure. In particular, we run a large number of Monte-Carlo simulations in which we destroy the intrinsic SDSS clustering by randomizing the supergalactic coordinates of the clusters while keeping their distances and therefore their selection function unchanged. On this intrinsically random cluster distribution, we apply the procedure described before and identify the expected random superclusters, N_{ran} , which are due to our supercluster-identification method itself.

In figure 3 (top panel) we plot for the different percolation radii, the probability of detecting real clusters in the SDSS data, defined as $\mathcal{P} = 1 - N_{\text{ran}}/N_{\text{SDSS}}$ as well as the number of real, N_{SDSS} (continuous line), and random, N_{ran} (dashed line), superclusters. In the pres-

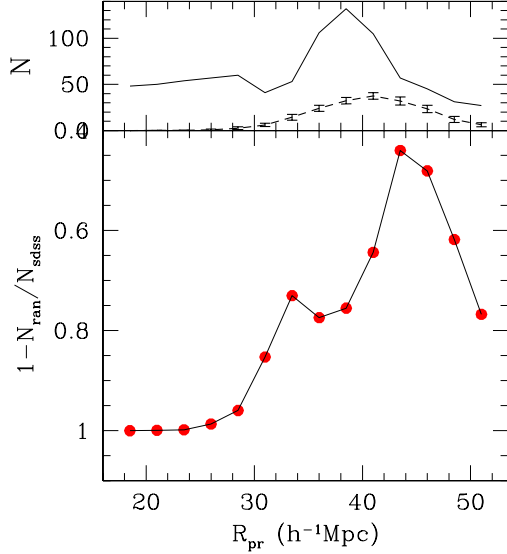


Figure 3. Statistical significance of our supercluster detection procedure as a function of percolation radius R_{pr} . Up panel shows the number of real, N_{SDSS} (continuous line), and random, N_{ran} (dashed line), superclusters respectively. Top panel shows the corresponding probability of detecting real superclusters in the SDSS data. Note that this plot accounts for clumps with at least eight cluster members.

ence of negligible systematic biases in our method and data, the above selection process should result in $\mathcal{P} \simeq 1$. In other words, the closer \mathcal{P} is to 1 the less likely to reveal random superclusters. To this end from figure 3 it is evident that with a threshold of $26 h^{-1}\text{Mpc}$ for the percolation radius, we find an average of 0.4 random superclusters in the mock SDSS realizations. Thus the superclusters we detect in the SDSS with $R_{pr} = 26 h^{-1}\text{Mpc}$ are significant at the $\geq 99\%$ confidence level. This is why we set this percolation threshold.

3.3 The Supercluster Global Geometry

Shapes are estimated for those superclusters that consist of 8 or more clusters * , utilizing the moments of inertia (I_{ij}) method to fit the best triaxial ellipsoid to the data (cf. Plionis, Barrow & Frenk 1991). We diagonalize the inertia tensor

$$\det(I_{ij} - \lambda^2 M_3) = 0 \quad (M_3 \text{ is } 3 \times 3 \text{ unit matrix}), \quad (1)$$

obtaining the eigenvalues $\alpha_1, \alpha_2, \alpha_3$ (where α_1 is the semi-major axis) from which we define the shape of the configuration since, the eigenvalues are directly related to the three principal axes of the fitted ellipsoid

$$\mathbf{r}(\theta, \phi) = a_1 \sin\theta \cos\phi \hat{\mathbf{i}} + a_2 \sin\theta \sin\phi \hat{\mathbf{j}} + a_3 \cos\theta \hat{\mathbf{k}}, \quad (2)$$

* In Kolokotronis et al. (2002), we have tested the performance of the shape method using a large set of Monte Carlo simulations (see their section 3.3) and they found that structures with more than 8 members (points) are well described by the our shape method.

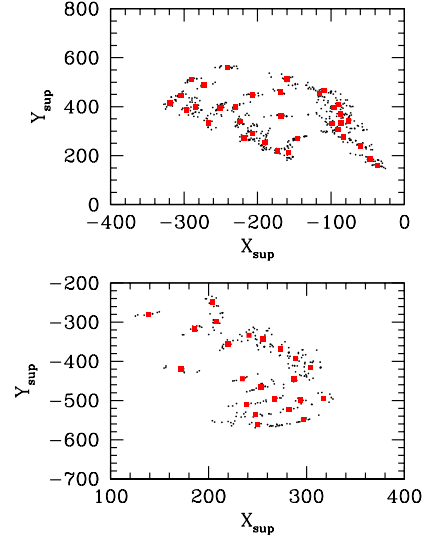


Figure 4. Two dimensional ($Z_{\text{sup}} = 0$) whole sky map of the 57 SDSS superclusters (squares). Dots denote the clusters associated with superclusters with $k \geq 8$. In this distribution we have detected 34 superclusters in the North and 23 in the South.

having volume $V = \frac{4\pi}{3} \alpha_1 \alpha_2 \alpha_3$ and $0 \leq \phi \leq 2\pi$, $0 \leq \theta \leq \pi$. The shape statistic procedure, that we use, is based on a differential geometry approach, introduced by Sahni et al. (1998). In this paper we review only some basic concepts.

Furthermore, having identified superclusters with $k \geq 8$ members a set of three shapefinders are defined having dimensions of length; $\mathcal{H}_1 = VS^{-1}$, $\mathcal{H}_2 = SC^{-1}$ and $\mathcal{H}_3 = C$, with S the surface area and C the integrated mean curvature. In this framework, based on these, the dimensionless shapefinders K_1 and K_2 can be defined as follows:

$$K_1 = \frac{\mathcal{H}_2 - \mathcal{H}_1}{\mathcal{H}_2 + \mathcal{H}_1} \quad (3)$$

and

$$K_2 = \frac{\mathcal{H}_3 - \mathcal{H}_2}{\mathcal{H}_3 + \mathcal{H}_2}, \quad (4)$$

where $K_{1,2} \leq 1$ by definition and normalized to give $\mathcal{H}_i = R$ ($K_{1,2} = 0$) for a sphere of radius R . The above shape vector $\mathbf{K} = (K_1, K_2)$ characterizes the shapes of topologically non-trivial cosmic objects according to the following classification: (i) pancake-like ellipsoids for $K_1 > K_2$ or $\mathcal{R} = K_1/K_2 > 1$; (ii) filament-like ellipsoids for $K_1 < K_2$ or $\mathcal{R} = K_1/K_2 < 1$; (iii) triaxial for $K_1 = K_2$ or $\mathcal{R} = K_1/K_2 = 1$ and (iv) spheres for $\alpha_1 = \alpha_2 = \alpha_3$ and thus $(K_1, K_2) = (0, 0)$. Note that for ideal filaments $\mathbf{K} = (0, 1)$, pancakes $\mathbf{K} = (1, 0)$, triaxial structures $\mathbf{K} = (1, 1)$ and spheres $\mathbf{K} = (0, 0)$.

For the quasi-spherical objects, K_1 and K_2 are both very small (order of $\sim 10^{-3} - 10^{-4}$), and thus the ratio $\mathcal{R} = K_1/K_2$ measures the deviation from pure sphericity (for further details see Basilakos et al. 2001). It is interesting to mention that in the present work we didn't find such small values for the (K_1, K_2) [for further details see next section].

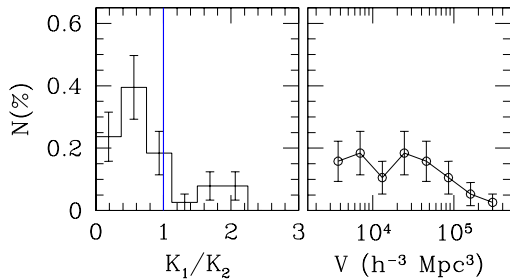


Figure 5. The shape and volume spectrum of the SDSS superclusters. The error-bars are estimated utilizing Poisson statistics

4 MORPHOLOGICAL PROPERTIES

We investigate supercluster characteristics according to the observational requirements and the definitions of shape statistic set in section 3. Taking the optimum value of $R_{\text{pr}} = 26h^{-1}$ Mpc for the combined SDSS sample, we find 57 superclusters with $k \geq 8$. Table 1, lists all the relevant information. In figure 4, we show a 2D ($Z_{\text{sup}} = 0$) schematic representation of superclusters (squares) and the related cluster distribution (dots) for the SDSS sample. Note, that only superclusters with $k \geq 8$ and their member clusters are plotted.

As is evident from Table 1, there are 19 entries which are near the boundaries of the SDSS cluster catalog. Therefore, in order to avoid ill shape definitions, for the shape statistics, we feel more secure to use superclusters which are away from the boundaries. This selection procedure decreases the total number of analysed entries to 38.

Again from Table 1, it is obvious that there are no spherical superclusters in concordance with numerical N-body simulations of gravitational clustering and similar studies on observed data (Plionis, Valdarnini & Jing 1992; Sathyaprakash et al. 1998a, b; Sahni et al. 1998; Basilakos et al. 2001; Kolokotronis et al. 2002). We plot in figure 5 the shape-spectrum as well as the multiplicity function (volume spectrum). The shape spectrum shows a measure of the global SDSS superclusters geometry. It is obvious that filamentary structures dominate our supercluster sample, in agreement with previous studies (Sathyaprakash et al. 1998a,b; Basilakos et al. 2001; Kolokotronis et al. 2002). It is interesting to mention that the vast majority of the systems (71% or 27/38) reveal filamentary configuration with 2 of them being close to pure triaxial $K_1 \simeq K_2$ or $\mathcal{R} \simeq 1$ (see Table 1: supercluster 31 and 44). The rest of the objects (11 or 29%) are estimated to be pancakes, with 3 of them being close to pure triaxial (see Table 1: supercluster 17, 18 and 54). The mean value of the semi-major supercluster axes is $\bar{\alpha}_1 = 54.96 \pm 22.34 h^{-1}$ Mpc. However, for the total supercluster sample we find 79% (45/57) filaments and 21% (12/57) pancakes respectively. Finally, the histogram in figure 6 presents the total number of the rich SDSS superclusters as a function of redshift corresponds to a mean density of order $\simeq 5.58(\pm 0.74) \times 10^{-6} h^3 \text{Mpc}^{-3}$.

A recent paper by Einasto et al. (2002) examines clusters and superclusters in the SDSS survey. Super-

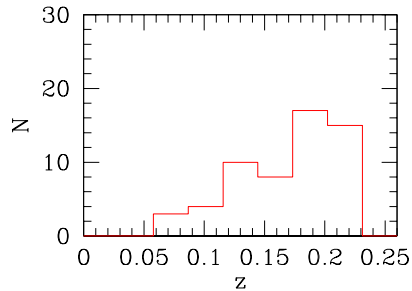


Figure 6. The number of the SDSS superclusters as a function of redshift.

clusters are found by these authors utilizing a smoothed apparent magnitude limited sample rather than the point distribution of clusters and the paper concentrates on measuring the high density regions. These authors found 43 superclusters, 35 of which are dubbed as rich ($k \geq 8$) up to redshift 0.2; we find 42 such superclusters. The smoothing technique owing to the coupling between the selection function and the constant radius smoothing could produce a distorted smoothed density distribution, especially at large distances (see Gaztanaga & Yokoyama 1993; Basilakos et al. 2001).

5 CONCLUSIONS

We have studied the morphological parameters of superclusters identified in the optical SDSS cluster catalog, up to redshift 0.23, using the selection features of the SDSS cluster catalog. We have applied a constant size percolation radius R_{pr} in order to detect superclusters within a distance where the cluster sample is volume limited. The measure of the global supercluster geometry has been based on a differential geometry method derived by Sahni et al. (1998) and we find that filaments (71%) dominate over pancakes (29%), in agreement with other recent large-scale structure studies.

ACKNOWLEDGEMENTS

This work is jointly funded by the European Union and the Greek Government in the framework of the programme 'Promotion of Excellence in Technological Development and Research', project 'X-ray Astrophysics with ESA's mission XMM'. Finally, I would like to thank the anonymous referee, for his/her useful suggestions.

REFERENCES

- Babul, A. & Starkman, G. D., 1992, ApJ, 401, 28
- Bahcall N., Soneira R., 1984, ApJ, 277, 27
- Bahcall N., Ann. Rev. Astr. Ap., 1988, 26, 631
- Basilakos S., Plionis M., Rowan-Robinson M., 2001, MNRAS, 223, 47 (BPR)
- Coles, P. & Plionis, M., 1991, MNRAS, 250, 75
- de Lapparent V., Geller M. J., Huchra J. P., 1991, ApJ, 369, 273

Table 1. List of the SDSS superclusters using $R_{\text{pr}} = 26h^{-1}$ Mpc. The correspondence of the columns is as follows: index number (the first 34 superclusters belong to the North and the rest of them in the South slice respectively), multiplicity, axes of triaxial ellipsoid, redshift, right ascension RA and declination DEC of the supercluster center, K_1 and K_2 are the shapefinders, their ratio $\mathcal{R} = K_1/K_2$ and finally the morphological classification type. F denotes filaments, P is for pancakes and cT is close to triaxial. Note that the index B, wherever exists, means that the specific entry is close to the boundaries of the SDSS cluster catalog. Finally, The a_1 , a_2 and a_3 have units of h^{-1} Mpc.

Index	k	α_1	α_2	α_3	z	RA	DEC	K_1	K_2	\mathcal{R}	Type
1	18	56.20	24.15	21.02	0.083	154.00	0.20	0.045	0.097	0.46	F-B
2	17	34.79	15.87	12.69	0.219	151.45	-0.07	0.048	0.093	0.52	F-B
3	16	42.80	20.95	15.71	0.196	149.62	0.01	0.050	0.084	0.59	F-B
4	15	44.06	19.04	16.89	0.106	154.48	0.47	0.043	0.094	0.46	F-B
5	10	36.23	16.89	12.59	0.162	149.78	-0.04	0.054	0.095	0.56	F-B
6	9	33.46	15.13	13.12	0.072	151.58	0.15	0.042	0.086	0.48	F-B
7	14	48.41	22.58	18.31	0.174	150.99	-0.24	0.046	0.087	0.52	F-B
8	21	81.49	35.79	30.22	0.207	153.96	0.07	0.046	0.096	0.48	F-B
9	10	46.67	21.31	18.05	0.185	151.47	-0.36	0.043	0.087	0.49	F-B
10	13	29.85	13.34	8.80	0.128	160.11	0.26	0.072	0.117	0.62	F
11	12	64.82	25.43	19.10	0.219	161.52	0.01	0.064	0.136	0.47	F
12	10	37.47	16.39	10.96	0.140	160.07	0.11	0.072	0.121	0.60	F
13	23	91.56	39.49	35.15	0.150	154.03	-0.14	0.043	0.094	0.46	F-B
14	24	79.67	31.36	28.34	0.116	160.16	0.02	0.048	0.113	0.42	F
15	8	37.02	10.08	9.07	0.185	169.56	-0.24	0.068	0.218	0.31	F
16	12	69.15	8.23	2.12	0.139	184.68	-0.45	0.375	0.610	0.62	F
17	11	48.46	11.00	2.36	0.219	180.92	0.18	0.430	0.410	1.05	cT
18	10	43.75	8.08	1.33	0.174	184.71	-0.23	0.514	0.481	1.07	cT
19	22	49.41	12.22	10.13	0.105	199.04	-0.08	0.078	0.261	0.30	F
20	12	42.01	14.24	3.95	0.208	202.48	-0.40	0.315	0.261	1.20	P
21	10	46.92	14.78	6.72	0.196	200.96	-0.41	0.171	0.251	0.68	F
22	16	69.95	15.87	11.76	0.162	204.20	-0.16	0.093	0.306	0.30	F
23	22	75.40	15.70	10.55	0.174	214.47	0.22	0.110	0.350	0.31	F
24	33	109.75	11.87	2.42	0.128	225.89	-0.14	0.454	0.640	0.71	F
25	21	78.94	16.00	11.65	0.151	215.41	-0.25	0.099	0.350	0.28	F
26	30	84.15	9.36	1.28	0.139	222.32	-0.11	0.582	0.640	0.91	F
27	26	65.28	8.71	5.55	0.105	226.05	-0.12	0.130	0.510	0.25	F-B
28	12	36.51	11.12	2.00	0.208	219.10	-0.20	0.470	0.311	1.50	P
29	23	78.40	12.78	6.92	0.196	224.02	0.25	0.160	0.460	0.34	F
30	16	37.64	12.57	6.75	0.219	227.71	-0.25	0.130	0.220	0.59	F-B
31	9	22.89	8.52	3.23	0.151	232.34	0.27	0.211	0.220	0.96	cT-B
32	9	33.08	11.50	2.06	0.208	229.53	0.29	0.462	0.270	1.71	P-B
33	12	44.35	10.41	8.02	0.185	231.34	0.13	0.088	0.290	0.30	F-B
34	12	30.66	9.74	6.12	0.117	230.55	0.06	0.101	0.220	0.47	F-B
35	29	121.03	17.30	12.13	0.219	2.86	0.11	0.114	0.474	0.24	F
36	10	58.86	13.48	9.95	0.163	357.00	-0.02	0.093	0.303	0.31	F-B
37	16	79.83	14.40	4.07	0.209	6.04	0.02	0.336	0.471	0.71	F
38	11	44.19	10.74	3.01	0.197	7.00	0.06	0.330	0.370	0.89	F
39	8	37.58	12.97	9.31	0.175	17.16	0.03	0.077	0.180	0.44	F
40	18	61.42	17.56	10.72	0.186	20.94	-0.25	0.111	0.253	0.44	F
41	10	66.06	8.82	4.79	0.072	11.27	0.02	0.159	0.530	0.30	F
42	10	32.35	14.59	2.80	0.198	18.64	0.12	0.420	0.193	2.17	P
43	8	46.06	8.43	7.45	0.107	12.01	-0.02	0.084	0.354	0.24	F
44	11	36.85	12.42	4.51	0.220	18.29	0.28	0.240	0.250	0.96	cT
45	8	35.27	7.06	1.20	0.209	18.72	0.19	0.502	0.453	1.11	P
46	11	45.26	12.57	8.28	0.129	25.72	0.04	0.100	0.253	0.40	F
47	9	39.60	14.05	2.30	0.220	34.21	0.03	0.491	0.266	1.84	P
48	14	44.69	15.31	11.82	0.152	32.15	-0.28	0.069	0.170	0.41	F
49	15	71.83	14.17	7.63	0.140	41.25	0.09	0.151	0.393	0.38	F
50	8	45.36	15.09	11.86	0.197	34.15	0.20	0.069	0.180	0.39	F
51	9	37.99	6.19	2.93	0.209	27.32	-0.15	0.190	0.472	0.39	F
52	19	36.46	10.30	1.57	0.197	44.74	0.14	0.527	0.340	1.55	P
53	24	68.23	16.56	0.70	0.209	44.43	0.08	0.835	0.402	2.08	P
54	11	31.04	11.20	3.78	0.186	45.22	0.22	0.250	0.235	1.07	cT
55	20	55.01	13.62	6.21	0.174	46.07	0.01	0.182	0.330	0.55	F-B
56	8	25.87	8.36	1.09	0.163	43.59	0.13	0.570	0.300	1.90	P
57	8	20.44	7.39	4.80	0.141	53.12	0.00	0.090	0.173	0.51	F-B

- Einasto M., Tago E., Einasto J., Andernach H., 1997, A&AS, 123, 119
- Einasto M., Einasto J., Tago E., Mueller V., Andernach H., 2001, AJ, 122, 2222
- Einasto J., et al., 2002, A&A submitted, astro-ph/0212312
- Frisch P. et al., 1995, A&A, 296, 611
- Goto, T., et al., 2002, AJ, 123, 1825
- Hoyle, F., Vogeley, M. S., Gott, J., 2002, MNRAS, 332, 311
- Hoyle, F., Vogeley, M. S., Gott, J., R., Blanton, M., Tegmark, M., Weinberg, D. H., Bahcall, N., Brinkmann, J., York, D. , 2002, ApJ, 580, 663
- Jatush, V. S., Sahni V., Shandarin S.F., Sathyaprakash B. S., 2003, MNRAS, in press, astro-ph/0302596
- Kerscher M. et al., 1997, MNRAS, 284, 73
- Kerscher M., Mecke K., Schmalzing J., Beisbart C., Buchert T., Wagner H., 2001a, A&A, 373, 1
- Kerscher M. et al., 2001b, A&A, 377, 1
- Kolokotronis, V., Basilakos, S., Plionis M., 2002, MNRAS, 331, 1020
- Luo, S. & Vishniac, E. T., 1995, ApJS, 96, 429
- Mecke K., Buchert T., Wagner H., 1994, A&A, 288, 697
- Plionis M., Barrow J.D., Frenk C.S., 1991, MNRAS, 249, 662
- Plionis M., Valdarnini R., Jing Y. P., 1992, ApJ, 398, 12
- Sahni V. & Coles P., 1995, Phys. Rep., 262, 1
- Sahni V., Sathyaprakash B. S., Shandarin S.F., 1998, ApJ, 495, L5
- Sathyaprakash B.S., Sahni V., Shandarin S.F., Fisher B. K., 1998a, ApJ, 507, L109
- Sathyaprakash B.S., Sahni V., Shandarin S.F., 1998b, ApJ, 508, 551
- Stoughton, C., et al., 2002, AJ, 123, 485
- Weinberg, D.H., Gott J.R. III, & Melott, A.L., 1987, ApJ, 321, 2
- West J. M., 1989, ApJ, 347, 610
- Yess C. & Shandarin S.F., 1996, ApJ, 465, 2
- Zeldovich, Ya. B., Einasto, J., Shandarin, S., 1982, Nature, 300, 407

Shape statistics of Sloan Digital Sky Survey superclusters

Spyros Basilakos¹.

¹ *Institute of Astronomy & Astrophysics, National Observatory of Athens, I. Metaxa & V. Pavlou, Palaia Penteli, 15236 Athens, Greece*

3 June 2003

ABSTRACT

We study the supercluster shape properties of the recently compiled SDSS cluster catalog using an approach based on differential geometry. We detect superclusters by applying the percolation algorithm to observed cluster populations, extended out to $z_{\max} \leq 0.23$ in order to avoid selection biases. We utilize a set of shapefinders in order to study the morphological features of superclusters with ≥ 8 cluster members and find that filamentary morphology is the dominant supercluster shape feature, in agreement with previous studies.

Keywords: cosmology: theory - clusters - superclusters: general - large-scale structure of universe - Optical: clusters

1 INTRODUCTION

The launch of the recent observational data has brought great progress in understanding the cosmic structure formation pattern. From the large scale structure point of view it has been shown that cluster of galaxies are not randomly distributed but tend to aggregate in larger groups, the so called superclusters (cf. Bahcall 1988). Since they have been seeded by density perturbations of the largest scale ($\sim 100 h^{-1}\text{Mpc}$), they therefore constitute objects with which one can study the details of the fluctuations that gave rise to cosmic structures (cf. West 1989; Einasto et al. 1997). In this framework, we can extract useful information regarding the evolution of the large-scale structure of the universe and test cosmological models within the framework of hierarchical structure formation scenario (Bahcall & Soneira 1984; Bahcall 1988; Frisch et al. 1995).

Indeed many authors have confirmed that the large scale clustering pattern of galaxies is described well by a filamentary distribution (Zel'dovich, Einasto & Shandarin 1982; de Lapparent, Geller & Huchra 1991; Einasto et al. 2001). However, only recently (Sathyaprakash et al. 1998a; Basilakos, Plionis & Rowan-Robinson 2001; Kolokotronis, Basilakos & Plionis 2002) was any significance given to cosmological inferences from supercluster shape statistics claiming that a low matter density ($\Omega_m = 1 - \Omega_\Lambda = 0.3$) flat cosmological model (ΛCDM) fits the observational results at high significance level. Sathyaprakash et al. (1998a) and Basilakos et al. (2001) have used infrared galaxy samples (1.2 Jy and PSCz, respectively), whereas Kolokotronis, et al. (2002) considered Abell/ACO clusters.

A variety of geometrical and topological methods have been developed and applied to observational data in order to give qualitative and quantitative description

of large scale structure (cf. Weinberg, Gott & Melott 1987; Coles & Plionis 1991; Mecke et al. 1994; Sahni & Coles 1995; Yess & Shandarin 1996; Kerscher et al. 1997; Kerscher et al. 2001a, b; Hoyle, Vogeley & Gott 2002; Hoyle et al. 2003; Jatush et al. 2003 and references therein). Recently, a new technique was obtained by Sahni, Sathyaprakash & Shandarin (1998) based on the differential geometry (Minkowski functionals), in order to describe in detail the geometrically and topologically complex features of large scale structure. In its general form the Minkowski functionals have been shown to provide a better approximation to complex structures than the simple semi-axes procedures (Sathyaprakash, Sahni & Shandarin 1998b). For example, in cases where the matter distribution is one-dimensional but not along straight line, one is bound to get somewhat smaller signal for filamentarity from the Babul & Starkman (1992) and Luo & Vishniac (1995) statistics (semi-axes method). This problem is even more true for two dimensional structures.

The first time this new shapefinder technique was applied to astronomical data was in Basilakos et al. (2001), where it ascertained that the prominent feature of the large scale structures we see today is filamentarity, as it has also been observed in N-body simulations of gravitational clustering (Sathyaprakash et al. 1998b and references therein). In this paper we utilize the recently completed SDSS CE cluster catalog (Goto et al. 2002) in order: (i) to study whether we can reliably identify SDSS superclusters and measure their shape and size distribution and (ii) whether or not superclusters verify the dominance of filamentarity as the basic trait of large scale structure. A different analysis applied by Einasto et al. (2002), who identified clusters and 43 superclusters (high density regions) from the smoothed galaxy density

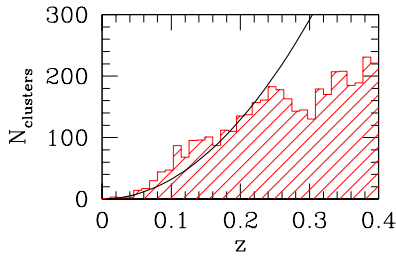


Figure 1. The estimated (histogram) and the expected (line) number of the SDSS clusters as a function of redshift.

field of the SDSS Early Data Release (Stoughton et al. 2002) catalog. The plan of the paper is as follows. The observed dataset is presented in section 2. In section 3, we give a brief report on the method used to investigate supercluster shape properties and comment on the systematic effects introduced in our analysis. In section 4, we present the morphological parameters of the SDSS superclusters data and finally in section 5 we draw our conclusions.

2 THE SDSS CLUSTER CATALOGUE

In the present analysis we use the recent SDSS CE cluster catalog (Goto et al. 2002), which contains 2770 and 1868 galaxy clusters in the North ($145.1^\circ < RA < 236.0^\circ$, $-1.25^\circ < DEC < 1.25^\circ$) and South ($350.5^\circ < RA < 56.61^\circ$, $-1.25^\circ < DEC < 1.25^\circ$) slices respectively, covering an area of $\sim 400\text{deg}^2$ in the sky. Redshifts are converted to proper distances using a spatially flat cosmology with $H_0 = 100h \text{ km s}^{-1} \text{ Mpc}^{-1}$ and $\Omega_m = 1 - \Omega_\Lambda = 0.3$. In figure 1, we present the estimated (histogram) and the expected (line) number of the SDSS clusters as a function of redshift. It is obvious that up to redshift $z_{\text{max}} \leq 0.23$ we have a volume limited sample due to the fact that the number of the SDSS clusters is proportional to r^3 . We have compare the two distributions (up to $z_{\text{max}} \leq 0.23$) via a standard Kolmogorov-Smirnov (KS) statistical test and the corresponding probability of consistency between model and observations is $\mathcal{P}_{\text{KS}} \simeq 0.43$. Therefore, the redshift cutoff corresponds to a limiting distance $r_{\text{max}} \leq 653h^{-1} \text{ Mpc}$. This subsample contains 1690 entries in the North and South slices respectively.

In order to investigate further the latter result we need to compute the number density of the cluster sample as a function of redshift. We do so by using five equal volume shells ($\delta V \approx 2.4 \times 10^6 h^{-3} \text{ Mpc}^3$) up to $z_{\text{max}} \leq 0.23$ and calculate, as a function of redshift, the cluster space density (continuous line in figure 2). While, the corresponding average-over-shells density for the SDSS subsample is $n_{\text{SDSS}}(\leq z_{\text{max}}) \simeq 1.26(\pm 0.32) \times 10^{-4} h^3 \text{ Mpc}^{-3}$ (see dashed line in figure 2) giving rise to intercluster separation of order $\sim 20 \pm 1.47 h^{-1} \text{ Mpc}$.

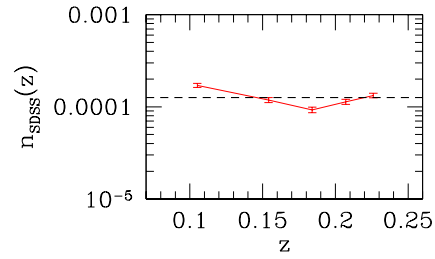


Figure 2. The SDSS cluster space density (continuous line) estimated in equal-volume shells with its Poissonian uncertainty. While the dashed line is the average $n_{\text{SDSS}}(z \leq 0.23) \simeq 1.26 \times 10^{-4} h^3 \text{ Mpc}^{-3}$.

3 SHAPE STATISTIC

3.1 SDSS Superclusters

Identifying real superclusters is a difficult problem in general, due to observational selection function, that can significantly affect the visual structure of superclusters and distort the true pattern. Our supercluster finding algorithm consists of the main steps: The supercluster catalogs constructed by utilizing, in supergalactic coordinates, a constant size neighborhood radius, i.e. the percolation radius (Zel'dovich et al. 1982). In particular, we place a sphere of a certain size around each cluster and then find all neighboring spheres having an overlap region. Then, all mutually linked clusters are joined together to form groups (with k members), and the groups with more than $k \geq 8$ clusters are identified as candidate rich superclusters. Of course, we choose the optimal percolation radius, by repeating the procedure by successively increasing the size of the sphere. At the end, we identify the radius that yields the maximum number of superclusters, which obviously occurs before the percolation of the superclusters themselves. Performing many tests we select a percolation radius $R_{\text{pr}} \simeq 26h^{-1} \text{ Mpc}$ following the same criteria to those of Einasto et al. (2001; Kolokotronis et al. 2002 and references therein). To this end this procedure produced a list of 57 rich superclusters.

3.2 Test for systematic errors

In this section we investigate the number of the random clumps revealed from the percolation procedure. In particular, we run a large number of Monte-Carlo simulations in which we destroy the intrinsic SDSS clustering by randomizing the supergalactic coordinates of the clusters while keeping their distances and therefore their selection function unchanged. On this intrinsically random cluster distribution, we apply the procedure described before and identify the expected random superclusters, N_{ran} , which are due to our supercluster-identification method itself.

In figure 3 (top panel) we plot for the different percolation radii, the probability of detecting real clusters in the SDSS data, defined as $\mathcal{P} = 1 - N_{\text{ran}}/N_{\text{SDSS}}$ as well as the number of real, N_{SDSS} (continuous line), and random, N_{ran} (dashed line), superclusters. In the pres-

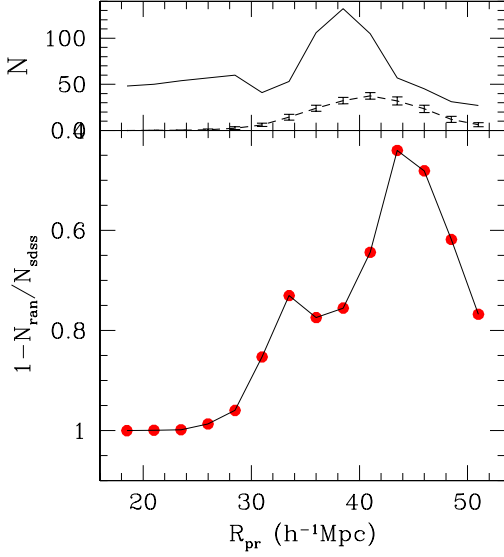


Figure 3. Statistical significance of our supercluster detection procedure as a function of percolation radius R_{pr} . Up panel shows the number of real, N_{SDSS} (continuous line), and random, N_{rand} (dashed line), superclusters respectively. Top panel shows the corresponding probability of detecting real superclusters in the SDSS data. Note that this plot accounts for clumps with at least eight cluster members.

ence of negligible systematic biases in our method and data, the above selection process should result in $\mathcal{P} \simeq 1$. In other words, the closer \mathcal{P} is to 1 the less likely to reveal random superclusters. To this end from figure 3 it is evident that with a threshold of $26h^{-1}\text{Mpc}$ for the percolation radius, we find an average of 0.4 random superclusters in the mock SDSS realizations. Thus the superclusters we detect in the SDSS with $R_{pr} = 26h^{-1}\text{Mpc}$ are significant at the $\geq 99\%$ confidence level. This is why we set this percolation threshold.

3.3 The Supercluster Global Geometry

Shapes are estimated for those superclusters that consist of 8 or more clusters^{*}, utilizing the moments of inertia (I_{ij}) method to fit the best triaxial ellipsoid to the data (cf. Plionis, Barrow & Frenk 1991). We diagonalize the inertia tensor

$$\det(I_{ij} - \lambda^2 M_3) = 0 \quad (M_3 \text{ is } 3 \times 3 \text{ unit matrix}), \quad (1)$$

obtaining the eigenvalues $\alpha_1, \alpha_2, \alpha_3$ (where α_1 is the semi-major axis) from which we define the shape of the configuration since, the eigenvalues are directly related to the three principal axes of the fitted ellipsoid

$$\mathbf{r}(\theta, \phi) = \alpha_1 \sin\theta \cos\phi \hat{\mathbf{i}} + \alpha_2 \sin\theta \sin\phi \hat{\mathbf{j}} + \alpha_3 \cos\theta \hat{\mathbf{k}}, \quad (2)$$

^{*} In Kolokotronis et al. (2002), we have tested the performance of the shape method using a large set of Monte Carlo simulations (see their section 3.3) and they found that structures with more than 8 members (points) are well described by the our shape method.

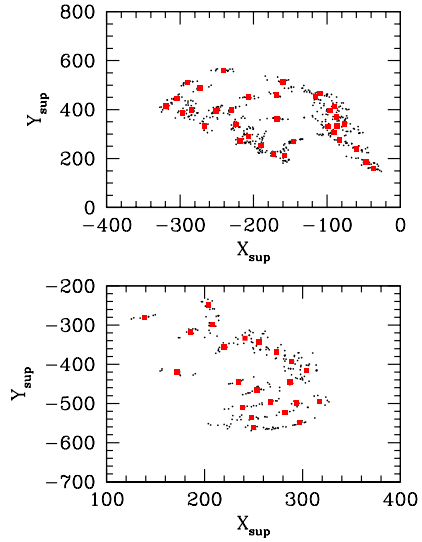


Figure 4. Two dimensional ($Z_{\text{sup}} = 0$) whole sky map of the 57 SDSS superclusters (squares). Dots denote the clusters associated with superclusters with $k \geq 8$. In this distribution we have detected 34 superclusters in the North and 23 in the South.

having volume $V = \frac{4\pi}{3} \alpha_1 \alpha_2 \alpha_3$ and $0 \leq \phi \leq 2\pi, 0 \leq \theta \leq \pi$. The shape statistic procedure, that we use, is based on a differential geometry approach, introduced by Sahni et al.(1998). In this paper we review only some basic concepts.

Furthermore, having identified superclusters with $k \geq 8$ members a set of three shapefinders are defined having dimensions of length; $\mathcal{H}_1 = VS^{-1}$, $\mathcal{H}_2 = SC^{-1}$ and $\mathcal{H}_3 = C$, with S the surface area and C the integrated mean curvature. In this framework, based on these, the dimensionless shapefinders K_1 and K_2 can be defined as follows:

$$K_1 = \frac{\mathcal{H}_2 - \mathcal{H}_1}{\mathcal{H}_2 + \mathcal{H}_1} \quad (3)$$

and

$$K_2 = \frac{\mathcal{H}_3 - \mathcal{H}_2}{\mathcal{H}_3 + \mathcal{H}_2}, \quad (4)$$

where $K_{1,2} \leq 1$ by definition and normalized to give $\mathcal{H}_i = R$ ($K_{1,2} = 0$) for a sphere of radius R . The above shape vector $\mathbf{K} = (K_1, K_2)$ characterizes the shapes of topologically non-trivial cosmic objects according to the following classification: (i) pancake-like ellipsoids for $K_1 > K_2$ or $\mathcal{R} = K_1/K_2 > 1$; (ii) filament-like ellipsoids for $K_1 < K_2$ or $\mathcal{R} = K_1/K_2 < 1$; (iii) triaxial for $K_1 = K_2$ or $\mathcal{R} = K_1/K_2 = 1$ and (iv) spheres for $\alpha_1 = \alpha_2 = \alpha_3$ and thus $(K_1, K_2) = (0, 0)$. Note that for ideal filaments $\mathbf{K} = (0, 1)$, pancakes $\mathbf{K} = (1, 0)$, triaxial structures $\mathbf{K} = (1, 1)$ and spheres $\mathbf{K} = (0, 0)$.

For the quasi-spherical objects, K_1 and K_2 are both very small (order of $\sim 10^{-3} - 10^{-4}$), and thus the ratio $\mathcal{R} = K_1/K_2$ measures the deviation from pure sphericity (for further details see Basilakos et al. 2001). It is interesting to mention that in the present work we didn't find such small values for the (K_1, K_2) [for further details see next section].

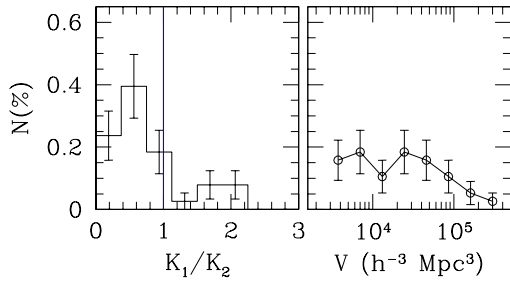


Figure 5. The shape and volume spectrum of the SDSS superclusters. The error-bars are estimated utilizing Poisson statistics

4 MORPHOLOGICAL PROPERTIES

We investigate supercluster characteristics according to the observational requirements and the definitions of shape statistic set in section 3. Taking the optimum value of $R_{pr} = 26h^{-1}$ Mpc for the combined SDSS sample, we find 57 superclusters with $k \geq 8$. Table 1, lists all the relevant information. In figure 4, we show a 2D ($Z_{sup} = 0$) schematic representation of superclusters (squares) and the related cluster distribution (dots) for the SDSS sample. Note, that only superclusters with $k \geq 8$ and their member clusters are plotted.

As is evident from Table 1, there are 19 entries which are near the boundaries of the SDSS cluster catalog. Therefore, in order to avoid ill shape definitions, for the shape statistics, we feel more secure to use superclusters which are away from the boundaries. This selection procedure decreases the total number of analysed entries to 38.

Again from Table 1, it is obvious that there are no spherical superclusters in concordance with numerical N-body simulations of gravitational clustering and similar studies on observed data (Plionis, Valdarnini & Jing 1992; Sathyaprakash et al. 1998a, b; Sahni et al. 1998; Basilakos et al. 2001; Kolokotronis et al. 2002). We plot in figure 5 the shape-spectrum as well as the multiplicity function (volume spectrum). The shape spectrum shows a measure of the global SDSS superclusters geometry. It is obvious that filamentary structures dominate our supercluster sample, in agreement with previous studies (Sathyaprakash et al. 1998a,b; Basilakos et al. 2001; Kolokotronis et al. 2002). It is interesting to mention that the vast majority of the systems (71% or 27/38) reveal filamentary configuration with 2 of them being close to pure triaxial $K_1 \simeq K_2$ or $\mathcal{R} \simeq 1$ (see Table 1: supercluster 31 and 44). The rest of the objects (11 or 29%) are estimated to be pancakes, with 3 of them being close to pure triaxial (see Table 1: supercluster 17, 18 and 54). The mean value of the semi-major supercluster axes is $\bar{\alpha}_1 = 54.96 \pm 22.34h^{-1}$ Mpc. However, for the total supercluster sample we find 79% (45/57) filaments and 21% (12/57) pancakes respectively. Finally, the histogram in figure 6 presents the total number of the rich SDSS superclusters as a function of redshift corresponds to a mean density of order $\simeq 5.58(\pm 0.74) \times 10^{-6}h^3\text{Mpc}^{-3}$.

A recent paper by Einasto et al. (2002) examines clusters and superclusters in the SDSS survey. Super-

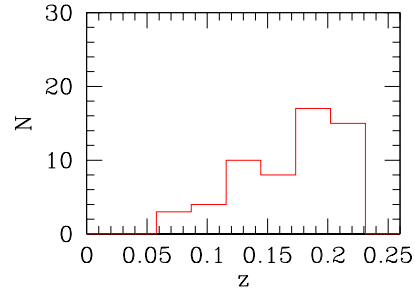


Figure 6. The number of the SDSS superclusters as a function of redshift.

clusters are found by these authors utilizing a smoothed apparent magnitude limited sample rather than the point distribution of clusters and the paper concentrates on measuring the high density regions. These authors found 43 superclusters, 35 of which are dubbed as rich ($k \geq 8$) up to redshift 0.2; we find 42 such superclusters. The smoothing technique owing to the coupling between the selection function and the constant radius smoothing could produce a distorted smoothed density distribution, especially at large distances (see Gaztanaga & Yokoyama 1993; Basilakos et al. 2001).

5 CONCLUSIONS

We have studied the morphological parameters of superclusters identified in the optical SDSS cluster catalog, up to redshift 0.23, using the selection features of the SDSS cluster catalog. We have applied a constant size percolation radius R_{pr} in order to detect superclusters within a distance where the cluster sample is volume limited. The measure of the global supercluster geometry has been based on a differential geometry method derived by Sahni et al. (1998) and we find that filaments (71%) dominate over pancakes (29%), in agreement with other recent large-scale structure studies.

ACKNOWLEDGEMENTS

This work is jointly funded by the European Union and the Greek Government in the framework of the programme 'Promotion of Excellence in Technological Development and Research', project 'X-ray Astrophysics with ESA's mission XMM'. Finally, I would like to thank the anonymous referee, for his/her useful suggestions.

REFERENCES

- Babul, A. & Starkman, G. D., 1992, ApJ, 401, 28
- Bahcall N., Soneira R., 1984, ApJ, 277, 27
- Bahcall N., Ann. Rev. Astr. Ap., 1988, 26, 631
- Basilakos S., Plionis M., Rowan-Robinson M., 2001, MNRAS, 223, 47 (BPR)
- Coles, P. & Plionis, M., 1991, MNRAS, 250, 75
- de Lapparent V., Geller M. J., Huchra J. P., 1991, ApJ, 369, 273

Table 1. List of the SDSS superclusters using $R_{\text{pr}} = 26h^{-1}$ Mpc. The correspondence of the columns is as follows: index number (the first 34 superclusters belong to the North and the rest of them in the South slice respectively), multiplicity, axes of triaxial ellipsoid, redshift, right ascension RA and declination DEC of the supercluster center, K_1 and K_2 are the shapefinders, their ratio $\mathcal{R} = K_1/K_2$ and finally the morphological classification type. F denotes filaments, P is for pancakes and cT is close to triaxial. Note that the index B, wherever exists, means that the specific entry is close to the boundaries of the SDSS cluster catalog. Finally, The a_1 , a_2 and a_3 have units of h^{-1} Mpc.

Index	k	α_1	α_2	α_3	z	RA	DEC	K_1	K_2	\mathcal{R}	Type
1	18	56.20	24.15	21.02	0.083	154.00	0.20	0.045	0.097	0.46	F-B
2	17	34.79	15.87	12.69	0.219	151.45	-0.07	0.048	0.093	0.52	F-B
3	16	42.80	20.95	15.71	0.196	149.62	0.01	0.050	0.084	0.59	F-B
4	15	44.06	19.04	16.89	0.106	154.48	0.47	0.043	0.094	0.46	F-B
5	10	36.23	16.89	12.59	0.162	149.78	-0.04	0.054	0.095	0.56	F-B
6	9	33.46	15.13	13.12	0.072	151.58	0.15	0.042	0.086	0.48	F-B
7	14	48.41	22.58	18.31	0.174	150.99	-0.24	0.046	0.087	0.52	F-B
8	21	81.49	35.79	30.22	0.207	153.96	0.07	0.046	0.096	0.48	F-B
9	10	46.67	21.31	18.05	0.185	151.47	-0.36	0.043	0.087	0.49	F-B
10	13	29.85	13.34	8.80	0.128	160.11	0.26	0.072	0.117	0.62	F
11	12	64.82	25.43	19.10	0.219	161.52	0.01	0.064	0.136	0.47	F
12	10	37.47	16.39	10.96	0.140	160.07	0.11	0.072	0.121	0.60	F
13	23	91.56	39.49	35.15	0.150	154.03	-0.14	0.043	0.094	0.46	F-B
14	24	79.67	31.36	28.34	0.116	160.16	0.02	0.048	0.113	0.42	F
15	8	37.02	10.08	9.07	0.185	169.56	-0.24	0.068	0.218	0.31	F
16	12	69.15	8.23	2.12	0.139	184.68	-0.45	0.375	0.610	0.62	F
17	11	48.46	11.00	2.36	0.219	180.92	0.18	0.430	0.410	1.05	cT
18	10	43.75	8.08	1.33	0.174	184.71	-0.23	0.514	0.481	1.07	cT
19	22	49.41	12.22	10.13	0.105	199.04	-0.08	0.078	0.261	0.30	F
20	12	42.01	14.24	3.95	0.208	202.48	-0.40	0.315	0.261	1.20	P
21	10	46.92	14.78	6.72	0.196	200.96	-0.41	0.171	0.251	0.68	F
22	16	69.95	15.87	11.76	0.162	204.20	-0.16	0.093	0.306	0.30	F
23	22	75.40	15.70	10.55	0.174	214.47	0.22	0.110	0.350	0.31	F
24	33	109.75	11.87	2.42	0.128	225.89	-0.14	0.454	0.640	0.71	F
25	21	78.94	16.00	11.65	0.151	215.41	-0.25	0.099	0.350	0.28	F
26	30	84.15	9.36	1.28	0.139	222.32	-0.11	0.582	0.640	0.91	F
27	26	65.28	8.71	5.55	0.105	226.05	-0.12	0.130	0.510	0.25	F-B
28	12	36.51	11.12	2.00	0.208	219.10	-0.20	0.470	0.311	1.50	P
29	23	78.40	12.78	6.92	0.196	224.02	0.25	0.160	0.460	0.34	F
30	16	37.64	12.57	6.75	0.219	227.71	-0.25	0.130	0.220	0.59	F-B
31	9	22.89	8.52	3.23	0.151	232.34	0.27	0.211	0.220	0.96	cT-B
32	9	33.08	11.50	2.06	0.208	229.53	0.29	0.462	0.270	1.71	P-B
33	12	44.35	10.41	8.02	0.185	231.34	0.13	0.088	0.290	0.30	F-B
34	12	30.66	9.74	6.12	0.117	230.55	0.06	0.101	0.220	0.47	F-B
35	29	121.03	17.30	12.13	0.219	2.86	0.11	0.114	0.474	0.24	F
36	10	58.86	13.48	9.95	0.163	357.00	-0.02	0.093	0.303	0.31	F-B
37	16	79.83	14.40	4.07	0.209	6.04	0.02	0.336	0.471	0.71	F
38	11	44.19	10.74	3.01	0.197	7.00	0.06	0.330	0.370	0.89	F
39	8	37.58	12.97	9.31	0.175	17.16	0.03	0.077	0.180	0.44	F
40	18	61.42	17.56	10.72	0.186	20.94	-0.25	0.111	0.253	0.44	F
41	10	66.06	8.82	4.79	0.072	11.27	0.02	0.159	0.530	0.30	F
42	10	32.35	14.59	2.80	0.198	18.64	0.12	0.420	0.193	2.17	P
43	8	46.06	8.43	7.45	0.107	12.01	-0.02	0.084	0.354	0.24	F
44	11	36.85	12.42	4.51	0.220	18.29	0.28	0.240	0.250	0.96	cT
45	8	35.27	7.06	1.20	0.209	18.72	0.19	0.502	0.453	1.11	P
46	11	45.26	12.57	8.28	0.129	25.72	0.04	0.100	0.253	0.40	F
47	9	39.60	14.05	2.30	0.220	34.21	0.03	0.491	0.266	1.84	P
48	14	44.69	15.31	11.82	0.152	32.15	-0.28	0.069	0.170	0.41	F
49	15	71.83	14.17	7.63	0.140	41.25	0.09	0.151	0.393	0.38	F
50	8	45.36	15.09	11.86	0.197	34.15	0.20	0.069	0.180	0.39	F
51	9	37.99	6.19	2.93	0.209	27.32	-0.15	0.190	0.472	0.39	F
52	19	36.46	10.30	1.57	0.197	44.74	0.14	0.527	0.340	1.55	P
53	24	68.23	16.56	0.70	0.209	44.43	0.08	0.835	0.402	2.08	P
54	11	31.04	11.20	3.78	0.186	45.22	0.22	0.250	0.235	1.07	cT
55	20	55.01	13.62	6.21	0.174	46.07	0.01	0.182	0.330	0.55	F-B
56	8	25.87	8.36	1.09	0.163	43.59	0.13	0.570	0.300	1.90	P
57	8	20.44	7.39	4.80	0.141	53.12	0.00	0.090	0.173	0.51	F-B

- Einasto M., Tago E., Einasto J., Andernach H., 1997, *A&AS*, 123, 119
- Einasto M., Einasto J., Tago E., Mueller V., Andernach H., 2001, *AJ*, 122, 2222
- Einasto J., et al., 2002, *A&A* submitted, astro-ph/0212312
- Frisch P. et al., 1995, *A&A*, 296, 611
- Goto, T., et al., 2002, *AJ*, 123, 1825
- Hoyle, F., Vogeley, M. S., Gott, J., 2002, *MNRAS*, 332, 311
- Hoyle, F., Vogeley, M. S., Gott, J., R., Blanton, M., Tegmark, M., Weinberg, D. H., Bahcall, N., Brinkmann, J., York, D., 2002, *ApJ*, 580, 663
- Jatush, V. S., Sahni V., Shandarin S.F., Sathyaprakash B. S., 2003, *MNRAS*, in press, astro-ph/0302596
- Kerscher M. et al., 1997, *MNRAS*, 284, 73
- Kerscher M., Mecke K., Schmalzing J., Beisbart C., Buchert T., Wagner H., 2001a, *A&A*, 373, 1
- Kerscher M. et al., 2001b, *A&A*, 377, 1
- Kolokotronis, V., Basilakos, S., Plionis M., 2002, *MNRAS*, 331, 1020
- Luo, S. & Vishniac, E. T., 1995, *ApJS*, 96, 429
- Mecke K., Buchert T., Wagner H., 1994, *A&A*, 288, 697
- Plionis M., Barrow J.D., Frenk C.S., 1991, *MNRAS*, 249, 662
- Plionis M., Valdarnini R., Jing Y. P., 1992, *ApJ*, 398, 12
- Sahni V. & Coles P., 1995, *Phys. Rep.*, 262, 1
- Sahni V., Sathyaprakash B. S., Shandarin S.F., 1998, *ApJ*, 495, L5
- Sathyaprakash B.S., Sahni V., Shandarin S.F., Fisher B. K., 1998a, *ApJ*, 507, L109
- Sathyaprakash B.S., Sahni V., Shandarin S.F., 1998b, *ApJ*, 508, 551
- Stoughton, C., et al., 2002, *AJ*, 123, 485
- Weinberg, D.H., Gott J.R. III, & Melott, A.L., 1987, *ApJ*, 321, 2
- West J. M., 1989, *ApJ*, 347, 610
- Yess C. & Shandarin S.F., 1996, *ApJ*, 465, 2
- Zeldovich, Ya. B., Einasto, J., Shandarin, S., 1982, *Nature*, 300, 407